Optics & Laser Technology 144 (2021) 107376

Contents lists available at ScienceDirect

Optics and Laser Technology

journal homepage: www.elsevier.com/locate/optlastec

Challenges in silicon photonics modulators for data center interconnect applications☆

Diego M. Dourado [a,*], Giovanni B. de Farias [b,c], Rodrigo H. Gounella [a], Mônica de L. Rocha [a], J. P. Carmo [a]

[a] Group of Metamaterials, Microwaves and Optics (GMeta), Electrical and Computing Engineering Department, EESC, USP, São Carlos, São Paulo, Brazil
[b] VLC Photonics, Valencia, Spain
[c] Division of Optical Technologies, CPqD Foundation, Campinas, São Paulo, Brazil

ARTICLE INFO

Keywords:
Silicon photonics
Optical modulators
Figures-of-merit
Data center interconnect
Trade-off analysis

ABSTRACT

The exponential demand for bandwidth in data centers is on high alert with the increase in data traffic. In this scenario, the design of optical modulators is crucial for the continuous evolution of communication systems. For data center interconnect (DCI) applications, this mean that modulators should offer high bandwidth and low optical loss. In addition, devices must operate with low power consumption and be compatible with complementary metal–oxide–semiconductor (CMOS) processes for low-cost and large-scale manufacturing. These facts show the importance of advancement in Silicon (Si) modulators solutions, since they have the potential to fulfill all these requirements. However, designing a device that meets all these requirements at the same time is still challenging, because there are several trade-offs problems involved for which different Silicon modulators types are not yet able to solve. In this context, this paper reviews the challenges in Silicon photonics (SiPh) modulators for data center interconnect applications.

1. Introduction

The study of photonic components based on Silicon (Si) started around the 80's, and early developments addressed waveguides and optical switches. Initially, Si-manufactured waveguides had relatively low optical loss (< 15 dB cm^{-1}) at telecommunications wavelengths, 1.31 μm and 1.55 μm [1,2]. Despite notable advances in Silicon photonics (SiPh) technology in the 1980s, little has been done to leverage a real integration of these technologies in the 1990s. Thanks to the substantial progress of SiPh and the idea of reusing Silicon-based technology platforms that are common in the microelectronics industry, the turning point came at the beginning of year 2000, when integration experiments began at the Silicon-on-insulator (SOI) and complementary metal–oxide–semiconductor (CMOS) foundries due to government investment [3]. Silicon photonics technology can enable the integration of several active and passive functionalities in a single photonic integrated circuit (PIC). A major advantage of SiPh circuits is its compatibility with CMOS processes, which enables monolithic integration with electronic circuits layers. In addition, CMOS technology delivers reliable and low-cost devices, which makes it promising for large-scale manufacturing. Nowadays, SiPh technologies are playing a crucial role in sustaining high data traffic demand, and have demonstrated high performance for optical interconnects.

With the incessant growing demand for services with high bandwidth and high speed, such as high-definition video streaming, cloud services including storage and software-as-a-service, besides the increasing number of mobile devices connected to internet, the traffic load in data centers is increasing exponentially. According to a Cisco forecast [4] for traffic growth from 2017 to 2022, the global internet protocol (IP) traffic will increase from 122 EB to 396 EB per month. Several IP video services, which includes IP video-on-demand (VoD), video files exchanged through file sharing, internet video, video conferencing, and video-streamed gaming, will account for about 80% to 90% of total IP traffic. In addition, the 2020 COVID pandemic has

☆ This work was supported in part by the Coordenação de Aperfeiçoamento de Pessoal de Nível Superior (Brazil, CAPES - Finance Code 001) and in part by the Fundação de Amparo à Pesquisa do Estado de São Paulo (Brazil, FAPESP - Finance Code 2016/20615-8).

* Corresponding author.
E-mail addresses: diego.dourado@usp.br (D.M. Dourado), gfarias@cpqd.com.br (G.B. de Farias), rodrigogounella@usp.br (R.H. Gounella), monica.rocha@usp.br (M. de L. Rocha), jcarmo@sc.usp.br (J.P. Carmo).

https://doi.org/10.1016/j.optlastec.2021.107376
Received 17 December 2020; Received in revised form 13 June 2021; Accepted 27 June 2021
Available online 16 July 2021

pushed the internet traffic even higher, due to the increase of home-office and remote work employees [5].

Due to this high demand for capacity, the development of technologies that meet bandwidth, energy consumption, cost and scalability requirements, is crucial. In this scenario, SiPh technologies are a promising solution to fulfill the growing demand for data center traffic, and have proven to be a compact alternative for the bulky classical optical devices that have become a bottleneck. SiPh devices emerges as a potential solution for future generations of optical communications systems, from short to long range applications [6]. Among these technologies, high-speed modulators are the key components for optical communication links. In general, modulation is performed directly by a laser or using an external modulator to modulate the output signal from a laser source. In the first case, the process is simpler and cheaper. However, external modulation is required to achieve high capacity with high information density in advanced high-order modulation formats. For this reason, advances in research related to electro-optical modulators are important. There are several platforms besides Si for the design of a modulator, e.g. Indium Phosphide (InP), Lithium Niobate ($LiNbO_3$), and polymer. Silicon has the advantage of being compatible with CMOS process, which leverages the large-scale manufacturing and high-reliability processes. According to a Yole Développement forecast [7], the market interest in Silicon photonics-based transceiver is expanding exponentially in the coming years. The total market for PIC-based transceivers using SiPh will grow from $0.45 B in 2018 to $4.14 B in 2024. This corresponds to a growth of 1.3 M to 23.5 M units. Thus, Silicon photonics-based transceivers will have a compound annual growth rate (CAGR) of 44.5% between the years 2018 and 2024.

Based on these two factors, i.e. high demand for data traffic and optical transceivers solutions, the improvement of optical modulators is required for future generations of transceivers, and several photonic devices configurations have been investigated to fulfill this need. The most popular types are based on $LiNbO_3$ modulators [8–10], InP modulators [11,12], Si *pn* junction modulators [13,14], and capacitive modulators [15,16]. Recent progress for high-speed and power-efficient devices has been demonstrated with Germanium-Silicon (GeSi)-based composition electro-absorption modulator (EAM) [17]. Typically, the modulator performance is assessed in terms of modulation efficiency ($V_\pi \times L$), insertion loss (IL) and electro-optical bandwidth (f_{3dB}). The device can be designed to operate in O-band (1.31 μm) or C-band (1.55 μm). Conventionally, for intra-data center interconnect (DCI) applications (links up to 10 km), modulators are designed to operate with on–off keying (OOK) format. For applications with 40 Gbit s^{-1} and 100 Gbit s^{-1} IEEE Ethernet standard, the OOK modulation has been widely applied. However, to provide greater capacity per channel, the 4-level pulse amplitude modulation (PAM-4) format was recently selected by the 400 Gbit s^{-1} (100 Gbit s^{-1} per channel) IEEE Ethernet standard [18] to support the high data flow. In this scenario, where the driver and optical amplifier are generally not used, the driving voltage should be $\leqslant$ 3.5 V [19] and the optical loss $\leqslant$5 dB. In terms of bandwidth, for 56 GBd applications, above 36 GHz for PAM-4 modulation is desirable [20]. On the other hand, for inter-DCI applications (links $>$ 10 km), coherent optical transmission is used with advanced modulation formats (e.g. quadrature phase-shift keying (QPSK) and high-order quadrature amplitude modulation (QAM)), and a higher driving voltage may be considered (e.g. 6.7 V [21]), since a driver amplifier is generally used.

For a better understanding of the challenges in Silicon modulators, the target high-level specifications is summarized below according to the requirements of future generations of optical transceivers. However, values are specified for intra-DCI applications, where energy consumption is critical due to the large number of connections over short distances.

- High modulation efficiency (V_π), with $V_\pi \leqslant 3.5$ V;
- Compact footprint (units of millimeter);
- Low optical insertion loss (IL), with IL$\leqslant$5 dB;
- High bandwidth (f_{3dB}), with $f_{3dB} \geqslant 36$ GHz;
- Low power consumption (units of pJ bit^{-1}).

Meeting these requirements for SiPh modulators is still challenging, because among all the high-level specifications listed, the main difficulty of Silicon modulators is to operate with low V_π and high bandwidth at the same time. Although there are some solutions in the state-of-the-art to perform this, in most cases, the modulator's complexity becomes a problem for large-scale and low-cost design. Therefore, in a simple and direct way, this paper aims to provide the challenges in SiPh modulators based on their limiting characteristics. Note that, the $V_\pi \leqslant 3.5$ V specification was chosen so that the device does not need a driver amplifier (lower power consumption). Regarding the waveguide length (L_{wg}), a short device is desired for low optical loss (given in dB m^{-1}) and simplicity of the transmission line design.

The paper is organized in four parts. Section 2 deals with fundamental concepts for evaluating the performance of SiPh modulators, and describes the main figures-of-merit (FOMs) for understanding the benefits and limitations of technology. In Section 3, a brief discussion of the physical effect for modulation with Silicon is presented. Based on this effect, the modulation mechanisms are presented together with a state-of-the-art analysis in Section 4, where the limiting characteristics for each technology are addressed. Finally, a brief conclusion is presented in Section 5.

2. Figures-of-merit

The performance of an optical modulator can be evaluated by several parameters, and the choice of a device can be associated with a specific application. Thus, some figures-of-merit, such as modulation depth (MD), bandwidth (f_{3dB}), insertion loss (IL), footprint and power consumption are characterized as the main performance characteristics of a modulator. Furthermore, one of the most used figures-of-merit to quantify the performance of an optical Silicon modulator is the modulation efficiency ($V_\pi \times L$), in which it evaluates the voltage V_π necessary to shift a wave in π radians at a given waveguide length (L_{wg}). For a better understanding of the modulators, the characteristics of each FOM mentioned in this paragraph will be discussed next.

2.1. Modulation depth

Several parameters are used to characterize optical signals, and most of them have specific limits. Extinction ratio (ER), also known as modulation depth (MD), is an important measure of the quality of an optical signal. This FOM is related to a variety of performance parameters of a modulation device. In most transmitters, even when in off-state, some power is emitted by the device. In the case of semiconductor lasers, for example, the off-state power (P_0) depends on the bias current (I_{bias}) and the threshold current (I_{th}). Therefore, if $I_{bias} < I_{th}$, the power emitted during the 0 transmission bit, P_0, is caused by spontaneous emission. Generally, P_0 is much lower than on-state power (P_1), with P_1 referring to 1 transmission bit. On the other hand, P_0 can be a significant fraction of P_1 depending on the biasing and driving conditions. Thus, the extinction ratio was defined in [22] as:

$$\mathrm{ER} = \frac{P_0}{P_1} \tag{1}$$

As in any communication system, there are noise sources to be taken into account. In this way, the signals can assume values determined with a certain probability, and the values of voltage or current can be modeled as continuous random variables. The decision limit value for each symbol can be associated with a Gaussian probability distribution with average current (I_1 and I_0) and standard deviation (δ_1 and δ_0) defined, for 1 and 0 bits, respectively. Therefore, a widely used method to measure the quality of a transmitted signal is through the eye diagram. To analyze the eye diagram, it is important to know that the

greater the eye opening, the better the transmitted signal quality. For this, the bit error rate (BER) expresses a ratio between the number of bits computed incorrectly and the total number of bits transmitted over a time period. This ratio can be obtained by setting the optimal decision limit using quality factor (Q) according to [22]. As noted at the beginning of this section (see Eq. (1)), an ideal value for P_0 would be zero. Thus, the optimal extinction ratio would be zero. Since in reality ER is not zero, the average power must be increased to maintain a constant value of Q and, as a result, a constant BER. This increase in transmitted power due to non-ideal extinction ratio values is defined as power penalty (δ_{ER}). Thus, the power penalty, given in dB, can be expressed as function of the extinction ratio [22].

$$\delta_{\mathrm{ER}} = 10\log_{10}\left(\frac{1+\mathrm{ER}}{1-\mathrm{ER}}\right) \tag{2}$$

Observing (2), it is concluded that a low extinction ratio is necessary to achieve a low power penalty. For intensity modulation, to improve the extinction ratio, P_0 must be minimized. However, if the driving signal amplitude is limited, this means that a decrease in P_0 also decreases the mean transmitted power, which increases optical loss. This leads to a trade-off problem between ER and optical losses.

2.2. Modulation bandwidth

Another important figures-of-merit for a modulator are bandwidth (f_{3dB}) and modulation speed (MS), i.e. a measurement of the amount of information that can be sent in the system. The bandwidth, given in Hz, can be calculated as the frequency range in which the spectral amplitude corresponds to 70.7% of its maximum value (or 50% of transmitted intensity). The term modulation speed is widely used for modulators to express the bit rate (given in bit s^{-1}) capacity that the device operates.

In optical modulators, modulation bandwidth depends on the electrode type, lumped or traveling-wave (TW), and the modulator capacitance per length, which depends on the radio-frequency (RF) dielectric constant and the geometry of the electrodes. For a lumped-type modulator, the bandwidth is limited by the optical or electrical transit time, whichever is smaller, or the time constant of the lumped-circuit parameters ($1/RC$), where R is the circuit resistance and C the capacitance of the modulator. In [23] a complete analytical model of small-signal electro-optical analysis is presented, in which a single-drive scheme to improve the modulator's electro-optical (EO) bandwidth, regardless of driving characteristic impedance, is addressed. For a traveling-wave modulator, the bandwidth is limited by the velocity mismatch between the optical and modulation waves, RF reflection coefficients, and the RF electrode loss. This problem can be solved by adjusting the phase velocity of the modulation signal to be equal to the phase velocity of the optical signal [24]. Therefore, the design of a TW-type transmission line is more complex than the design of a lumped-type transmission line. Studies in [25] show analytical techniques of equivalent circuits using coplanar waveguide (CPW) according to [26]. The model is based on carrier depletion modulators, and shows small-signal calculation techniques for high frequency electrical parameters as well as modulation bandwidth. Numerical methods with a similar approach were explored in [27].

2.3. Insertion loss

Since all external modulators have some insertion losses, a power loss occurs whenever an external modulator is used [22]. This problem can be minimized by designing a modulator for low losses in the desired wavelength. For Silicon modulators, losses occur mainly due to waveguide doping. In addition, the device's manufacturing process can also significantly increase optical loss.

The insertion loss (IL), given in dB, is the device optical loss when the modulator is inserted, at its maximum transmission intensity (I_m) value [28],

$$\mathrm{IL} = 10\log_{10}\left(\frac{I_t}{I_m}\right) \tag{3}$$

where I_t is the optical intensity that could be transmitted by the system if the modulator was absent.

2.4. Footprint

The dimensions of the device are crucial factors to improve the information density. Thus, Mach–Zehnder modulators (MZMs) based on the carrier depletion mechanism (to be explained in Section 4.2), for example, have relatively low modulation efficiency (high $V_\pi \times L$) and are therefore designed with long interaction lengths (in the order of millimeters) for lower driving voltages. On the other hand, resonant devices take advantage of this figure-of-merit, since the optical path can be increased without the need to expand the area of the equipment (e.g. ring resonator), and can be manufactured in smaller dimensions (in the order of micrometers). Silicon modulators with high modulation efficiency (low $V_\pi \times L$) also have this advantage of being designed in shorter lengths, behaving as lumped-type devices, and the RF voltage is considered instantaneously uniform along their electrodes.

In the case of a traveling-wave Mach–Zehnder interferometer (MZI) configuration, a long length affects bandwidth, insertion loss, and cost [29]. On the other hand, the optical bandwidth of resonant devices depends on the free spectral range (FSR), and tends to be more limited when compared to the bandwidth of interferometers. Modulators based on a MZI configuration can experience larger working wavelength range (> 40 nm) than resonant structures (~ 10 nm) [30].

2.5. Power consumption

Another important feature in this study is the electrical power consumption to operate the device. As reported in [28], the power required to operate the modulator depends on the modulation frequency, and can be measured by relating operating power per bandwidth unit. Usually, this figure-of-merit is expressed in J bit^{-1}. Currently, energy efficiency has stood out as one of the main metrics for interfaces involving photonic integrated circuit. In the case of EO modulators, power consumption depends on the physical properties of the phase-shifters and the design of the driving circuit layers. Fig. 1 outlines two typical examples for measuring power consumption in EO modulators.

Usually, TW-type modulators have 50 Ω input impedance (r_i) matched with 50 Ω transmission line and RF cables impedance (Z_L) in order to achieve maximum power transfer, and driving voltage (V_D) is only half the voltage of the open circuit source (V_0), as shown in Fig. 1a. In this case, for an OOK modulation format, the power consumption ($E_{bit,R}$) can be estimated by the power dissipation in the load resistor (R_L) during one slot duration (T_{bit}) [31].

$$E_{bit,R} = \frac{1}{4}\frac{V_D^2 T_{bit}}{R_L} \tag{4}$$

Consider $R_L = 50\ \Omega$, 100 ps bit duration, $V_D = 1$ V, and 10 Gbit s^{-1} bit rate, for example. From (4), the power consumption is 500 fJ bit^{-1} [31]. For a TW device, the power estimates assume that the power consumed by the charge–discharge cycle of the *pn* junction *RC* circuit is negligible.

On the other hand, this power consumption can be reduced by using lumped-type modulators. Such devices have higher modulation efficiency than TW-type modulators. For this reason, they can be manufactured with shorter lengths, behaving as lumped-element. In other words, the phase-shifter length of lumped-type modulators can be short compared to the RF wavelength of the modulation signal, so the device does not need to be designed in a TW configuration (longer length) with matched impedance. In this case, lumped-type devices can be operated

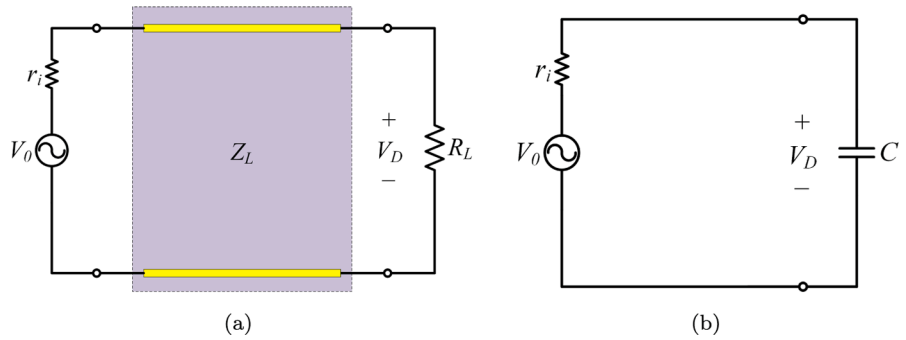

Fig. 1. Equivalent circuit for (a) TW-type modulators and (b) lumped-type modulators.

by purely capacitive loads, as shown in Fig. 1b. Considering a lumped-type modulator operating below its cut-off frequency (f_c),

$$f_c = \frac{1}{2\pi r_i C} \tag{5}$$

the driving voltage reaches a steady-state value equivalent to $V_D = V_0$. In this way, the power consumption will be related to the power dissipated in the resistor r_i during the charging and discharging of the capacitor with capacitance C. For a OOK or QPSK modulation format, the power consumption (E_{bit,C_1}) for these modulators is expressed in (6) [31]. For a high-order modulation format, such as 16-QAM, the power consumption (E_{bit,C_2}) is given in (7) [32].

$$E_{bit,C_1} = \frac{1}{4} V_D^2 C \tag{6}$$

$$E_{bit,C_2} = \frac{5}{72} V_D^2 C \tag{7}$$

Consider $V_D = 1$ V and 500 μm phase-shifter length, which has a capacitance of 200 fF, for example. From (6), the power consumption (E_{bit,C_1}) is 50 fJ bit^{-1} [31]. Note that, when compared to the previous example (TW-type modulator), the power consumption is 10x lower.

2.6. Modulation efficiency

The modulation efficiency ($V_\pi \times L$) is the most discussed FOM to assess the relation between the voltage V_π required to shift π radians between two optical waves and the optimum structure length (L_{wg}). This figure-of-merit is given in V m (in the order of V mm or V cm). Lithium Niobate ($LiNbO_3$) modulator has low voltage-induced phase change and low optical loss characteristics. For these reasons, this device is designed with a long length to achieve a π phase shift, and the use of modulation efficiency ($V_\pi \times L$) is not significant for quantifying its performance. On the other hand, the modulation efficiency is a relevant FOM to quantify the performance of Silicon modulators, since they have higher losses than the $LiNbO_3$ device and, therefore, are more limited in terms of length. In the case of modulators that have a Silicon waveguide, when subjected to a bias voltage (V_{bias}), the product $V_\pi \times L$ varies non-linearly due to the non-linear change of the Silicon refractive index. In this way, the FOM product can be calculated as [33]:

$$V_\pi \times L = \frac{\lambda}{2} \frac{dV_{bias}}{dn_{eff}} \tag{8}$$

where λ is the wavelength and dn_{eff} is the effective index variation caused by the bias voltage variation (dV_{bias}) applied to metal gate.

Regarding devices based on linear EO effect (Pockels effect), modulation efficiency varies linearly with the driving voltage applied to the structure. The phenomenon is observed thanks to the rearrangement of the crystalline structure that some materials have in the presence of an electric field and, consequently, a linear effective index variation of the material when exposed by an electric field.

3. Physical effect for optical modulation in silicon

Applying an electric field to a material may result in a change in the real refractive index (electro-refraction) and a change in the imaginary refractive index (electro-absorption). In semiconductors, the plasma dispersion effect is related to the density of free carriers. In this effect, the change in free carriers distribution varies the refractive index and absorption and, consequently, the phase and intensity of optical wave incident on the material. Observing Drude-Lorentz equations [34], changes in the absorption coefficient ($\Delta\alpha$) and refractive index (Δn_i) in the semiconductor can be related to changes in electrons (ΔN_e) and holes (ΔN_h) concentrations. Thus, $\Delta\alpha$ and Δn_i are represented in Eqs. (9) and (10),

$$\Delta\alpha = \frac{e^3\lambda_0^2}{4\pi^2 c^3 \epsilon_0 n_i}\left(\frac{\Delta N_e}{\mu_e m_e^2} + \frac{\Delta N_h}{\mu_h m_h^2}\right) \tag{9}$$

$$\Delta n_i = -\frac{e^2\lambda_0^2}{8\pi^2 c^3 \epsilon_0 n_i}\left(\frac{\Delta N_e}{m_e} + \frac{\Delta N_h}{m_h}\right) \tag{10}$$

where e is the electronic charge, λ_0 is the vacuum wavelength, c is the speed of light in vacuum, ϵ_0 is the vacuum permittivity, n_i is the material refractive index, μ_e is the electron mobility, μ_h is the hole mobility and, finally, m_e and m_h are the effective masses of electrons and holes, respectively.

The study in [35] performed the numerical integration of the experimental electro-absorption spectra with the doping spectra extracted from the literature, specifically in the wavelengths of 1.31 μm and 1.55 μm. Surprisingly, the results were consistent with the numerical model proposed by Drude-Lorentz. However, later on, they observed that the model fit only for electrons, and an adjustment of $N_h^{0.8}$ should be applied to the holes. Eqs. (11)–(14) are used to evaluate changes in the refractive index and absorption coefficient due to the change in charge concentration in Silicon [34]. According to (11) and (12), Fig. 2 shows an example of variation in the refractive index and absorption for Silicon, in which the doping concentration (ΔN_e and ΔN_h) was varied.

$$\Delta n_i|_{\lambda=1.55\ \mu m} = -8.8\times10^{-22}\Delta N_e - 8.5\times10^{-18}\Delta N_h^{0.8} \tag{11}$$

$$\Delta\alpha|_{\lambda=1.55\ \mu m} = 8.5\times10^{-18}\Delta N_e + 6\times10^{-18}\Delta N_h \tag{12}$$

$$\Delta n_i|_{\lambda=1.31\ \mu m} = -6.2\times10^{-22}\Delta N_e - 6\times10^{-18}\Delta N_h^{0.8} \tag{13}$$

$$\Delta\alpha|_{\lambda=1.31\ \mu m} = 6\times10^{-18}\Delta N_e + 4\times10^{-18}\Delta N_h \tag{14}$$

As the absorption coefficient change in Silicon is very low, Eqs. (11) and (13) are more relevant to the study of Si modulators, since it is possible to obtain viable performance with the refractive index change. Thus, using a MZI, for example, the optical phase shift can be converted into an optical intensity modulation. For a better understanding of

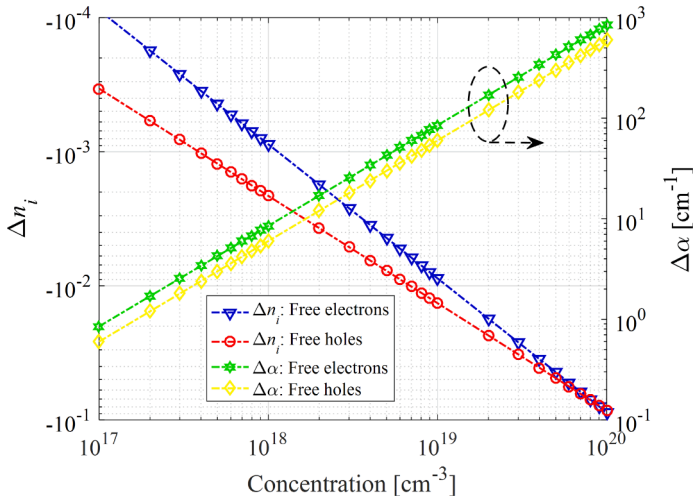

Fig. 2. Carrier refraction and absorption in Silicon as functions of concentration, when $\lambda = 1.55$ μm.

Table 1
Metric characteristics of optical modulation devices in SiPh circuits.

Ref.	Structure	Year	Mechanism	Figures-of-merit (FOMs)				
				ER [dB]	MS [Gbit s^{-1}]	IL [dB]	$V_\pi \times L$	
							L_{wg} [mm]	[V cm]
[36]	MZI	2004	carrier accumulation	> 16	1	~ 15.3	10	~ 8
[37]	MZI	2005	carrier accumulation	3.8	10	10	3.45	3.3
[38]	MZI	2013	carrier accumulation	3.6	15	2.2	0.2	0.3
[39]	MZI	2013	carrier accumulation	5	10	~ 3.7	NA	0.3
[40]	MZI	2014	carrier accumulation	~ 8	40	2.6	0.4	< 0.2
[41]	MZI	2016	carrier accumulation	NA	NA	5	2.5	0.5
[16]	MZI	2018	carrier accumulation	3.65	25	~ 26	0.5	1.53
[42]	MZI	2019	carrier accumulation	NA	> 8	~ 2.1	0.7	~ 1.08
[43]	Ring	2005	carrier injection	15	1.5	< 1	NA	NA
[44]	MZI	2005	carrier injection	NA	> 20	~ 4	5	0.5
[45]	MZI	2007	carrier injection	~ 8	10	12	0.2	0.036
[46]	Ring	2007	carrier injection	> 9	12.5	NA	NA	NA
[47]	Ring	2010	carrier injection	NA	1	< 0.1	NA	NA
[48]	MZI	2012	carrier injection	~ 8	12.5	~ 13.4	0.1	0.0155
[49]	MZI	2010	carrier depletion	6	12.5	2.5	1	1.4
[50]	MZI	2012	carrier depletion	6.6 3.2	40	6 4.5	4.7 0.95	3.5
[51]	MZI	2012	carrier depletion	> 7	50	~ 4.2	2.4	2.4
[52]	MZI	2012	carrier depletion	20 16 12.5	50 40 30	4.1 6.6 9	2 4 6	2.4 2.08 1.86
[53]	MZI	2012	carrier depletion	NA	> 24	< 20	2	0.7
[54]	MZI	2013	carrier depletion	4.4	60	3.5	0.75	< 2
[55]	MZI	2020	carrier depletion	> 25	> 50	5.9	2	1.2
[56]	MZI	2020	carrier depletion	~ 3	100	6.9	2.47	1.5

devices that use the plasma dispersion effect, Section 4 describes the main modulation mechanisms considering the state-of-the-art of SiPh modulators.

4. Silicon modulation mechanisms: A state-of-the-art analysis

As in the previous sections important characteristics of optical modulators were discussed, such as figures-of-merit and physical effect, in this section, several works related to optical modulators in SiPh circuits were selected, which show the evolution of devices with different techniques applied for increasing the performance. In this context, the analysis will be carried out on devices that use the plasma dispersion effect as modulation mechanism, explained previously in Section 3. Before presenting the modulation mechanisms, in Section 4.1, fundamental concepts of Si modulator designs will be presented, which relate the basic waveguide geometry with its main FOMs. Next, the following sections are divided according to the modulation mechanism type, i.e. carrier depletion (in Section 4.2), carrier injection (in Section 4.3) and carrier accumulation (in Section 4.4). For a better understanding of the modulation mechanisms, notable state-of-the-art references presented in Table 1, as well as several other studies that address the Si technology, will be discussed. For carrier-accumulation-based modulators, only purely Si & poly-crystalline Silicon (Poly-Si) were included in Table 1, since state-of-the-art hybrid devices will be discussed in Section 4.4.

4.1. Waveguide geometry and its impact on FOMs

This section deals with basic concepts of the impact of the modulator's geometry on its performance. For this, consider Figs. 3–5. Although each type of device configuration has its particularities, these general concepts are of fundamental importance in the modulator design.

With respect to the doping parameter, there is a trade-off between optical loss and bandwidth. To decrease the waveguide loss and the electrical access resistance between the RF signal and the waveguide, the modulator is generally designed with three doping levels (n/p, n_+/p_+, and n_{++}/p_{++}). If the high n_+/p_+ doping is too close to the waveguide, the optical loss will increase. However, the electrical access resistance will be lower, which improves the device bandwidth. To optimize this trade-off, the distance from the high-doped region to the waveguide (w) must be optimized. For this, it is suggested a study of (w vs. IL) and (w vs. f_{3dB}) to choose the best w point (typically between 100 nm and 800 nm) so that the modulator's operating requirements (IL and f_{3dB}) in a given system are satisfied.

Other important studies on the geometry of the modulator are the waveguide width (W), waveguide thickness (t) and slab thickness (t_{slab}). As it is necessary to avoid higher order modes, these parameters must be chosen so that a single propagation mode with high optical confinement propagates. This will result in high variation of the effective index (n_{eff}) for better performance of $V_\pi \times L$. In general, the silicon thickness is limited by the services offered in the foundry, e.g. typically SOI thickness of 220 nm, which makes W an important parameter for a target purpose. Parameter t_{slab} also impacts the speed of the device, since a thicker t_{slab} decreases the electrical access resistance (slabs with larger doped area), improving the bandwidth. However, this affects the loss and optical mode confinement in the waveguide, and a joint study between W, t, t_{slab}, and w must be performed.

4.2. Carrier depletion

Optical modulators based on the carrier depletion mechanism have some level of free carriers concentration in the waveguide when no voltage is applied through the *pn* junction. When a reverse bias voltage is applied to the junction, an electric field repels free carriers in the waveguide, creating a space charge region called the depletion region [57]. Through this effect, it is possible to change the device refractive index by varying the carriers concentration and, therefore, modulate the optical signal. Due to their nature of providing high bandwidth, depletion devices are extensively studied by researchers worldwide. However, they are not efficient in general, and require long phase-shifters to perform the optical signal modulation. To improve compatibility with high-speed CMOS devices, the main challenge of depletion modulators is to improve the figure-of-merit $V_\pi \times L$ while maintaining a low acceptable level of optical loss, since they will be able to operate with lower electric driving voltage and shorter active phase-shifter length.

Different configurations have been studied for years to improve depletion modulators [58,49,59,60,55,61,62,50]. Transceivers based on Silicon are already commercialized by several companies [63–67]. For example, a 3 mm carrier depletion modulator with $V_\pi \times L = 4$V cm, IL ≈ 7 dB, and $f_{3dB} > 20$ GHz was demonstrated [68]. Due to the improvement of these devices, for comparison, Table 1 presents more efficient solutions for telecommunication applications ($V_\pi \times L$ about 2x lower).

Fig. 3 shows three approaches to the active structure configuration, in which p and n represent the doped regions with their respective charge carriers, holes and electrons. The intrinsic Silicon region is represented by i.

Compared to electrons, holes have lower absorption but higher index change (see (11) and (13)). Therefore, it is common to use holes for offset-junction designs in Silicon modulators. Thus, an offset from the junction to the waveguide center is used to optimize $V_\pi \times L$. The dc bias voltage (V_{bias}) is another important parameter for the modulator design. In the case of depletion modulators, an increase in V_{bias} results in an increase in the effective index change and a decrease in the optical loss, since the carriers are removed from the waveguide. The increase in V_{bias} also impacts the cutoff frequency of the device, since the cutoff frequency increases due to the reduction in RC, a result of the expanded depletion region. If a long junction (high capacitance) and high source impedance are used (typically 50 Ω), the RC constant becomes a limiting parameter in the modulator's bandwidth. For this reason, TW electrodes are generally employed.

The *pn* junction [49,51–56] (see Fig. 3a) is the type of configuration most used for carrier-depletion-based phase-shifters. The reason for this

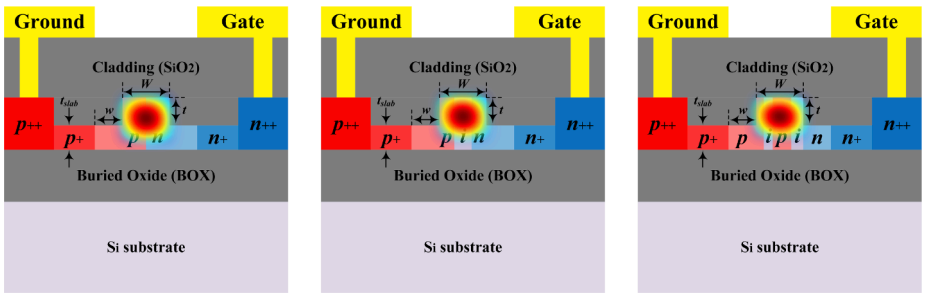

Fig. 3. Cross-section view of the Si phase-shifter with lateral (a) *pn* junction, (b) *pin* junction, and (c) *pipin* junction, for carrier-depletion-based modulators.

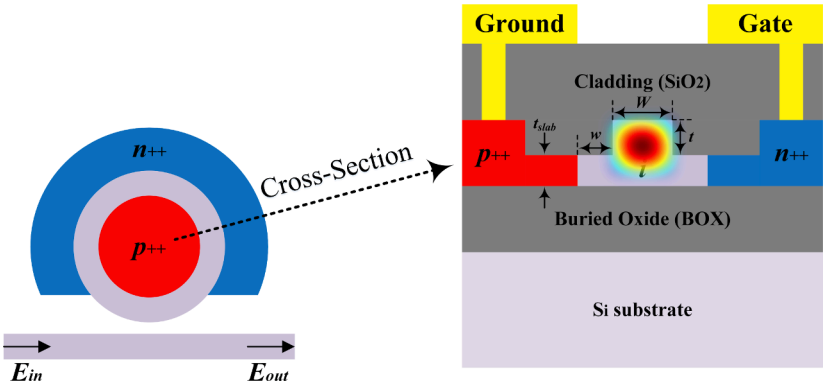

Fig. 4. *pin* junction embedded in a Silicon ring for carrier-injection-based modulators.

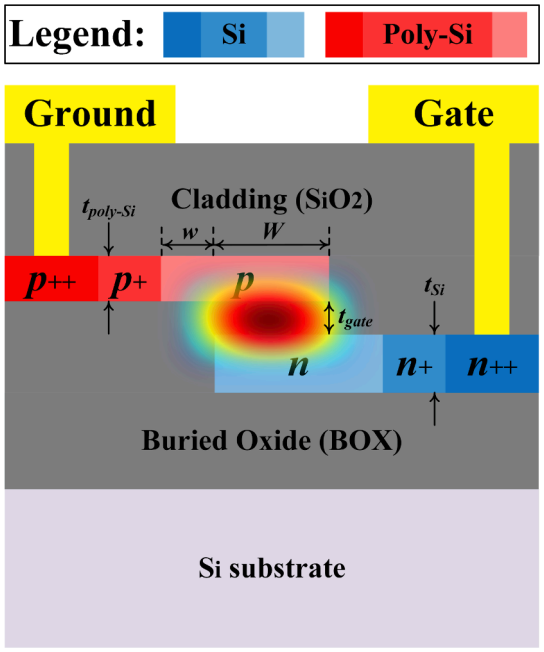

Fig. 5. Cross-section view of a carrier-accumulation-based traditional Si modulator.

comes from the higher modulation efficiency when compared to *pin* [62] and *pipin* [50] junctions (Figs. 3b and c, respectively). In fact, with a pure *pn* junction, it is possible to obtain higher change in the refractive index when the device is subjected to a bias voltage and, consequently, a lower value of $V_\pi \times L$. On the other hand, the *pn* configuration has higher optical loss when compared to junctions that have an intrinsic region, since its active area is fully doped with charge carriers. For depletion modulators, due to the diode behaviour of the junction, the depletion saturates for high voltages [69], which depends on the device geometry and doping concentrations. In addition, the effective index variation with the voltage is non-linear and starts to decrease as the applied voltage increases. Unlike lateral *pn* junction devices from Fig. 3, some vertical *pn* junction modulators [70] require electrical contact to the top of the waveguide, which results in a more complex growth process for manufacture. Vertical *pn* junction modulators with a better configuration for the electrical access and highly efficient ($V_\pi \times L < 1$V cm) have been demonstrated [71,69], however, the phase-shifter manufacturing process is still complex.

The idea of manufacturing a phase-shifter with intrinsic Silicon configuration came to minimize the modulator optical loss, since the phase-shifter's active area is not fully doped as the active area of a *pn* configuration. However, in a *pin* configuration, for example, the modulation efficiency is sacrificed. The *pipin* configuration was invented to optimize the trade-off between modulation efficiency and optical loss, because the doping is only present where the modulation effectively occurs. This solution is more complex to manufacture, since the central *p*-type region (see Fig. 3c) must be very narrow and requires accurate lithography. The *pipin* configuration has bandwidth similar to *pn*.

Regarding electrical behavior, carrier depletion modulators are designed with long lengths (in the order of millimeters) because they have relatively low modulation efficiency. This means that the modulator length is much longer ($>$ 10x) than the wavelength of the electric radio-frequency (RF) wave in the frequency range of tens of GHz. In this case, the RF electric wave travels through the modulator. This results in increasing the complexity of the modulator's design due to the RF lines design. Devices with these characteristics are known as traveling-wave (TW). For example, a typical TW-type depletion modulator that is available in a commercial foundry [72] has technical specifications of $V_\pi = 12$ V, IL $= 2.5$ dB, $f_{3dB} = 37$ GHz, and phase-shifter length of 1.5 mm. Although this device has low optical loss and acceptable bandwidth for DCI applications, the modulator has relatively low modulation efficiency when compared to capacitive and Silicon-organic hybrid (SOH) modulators, for example. This fact increases power consumption. In the literature, it is possible to show high modulation speed ($f_{3dB} > 40$ GHz) and loss $<$ 4 dB with such technology [27]. However, state-of-the-art devices are still very inefficient ($V_\pi \approx 8$ V), which makes it difficult to use them for short and medium range applications, where the energy consumption is critical.

Performing a general analysis of Table 1, we observed that carrier depletion modulators can offer high modulation speeds ($>$ 50 Gbit s^{-1} [51,52,54–56]). For this type of device, the manufacturing process is relatively simple and, for this reason, it has become the preferred modulator design in SiPh foundries. When compared to carrier injection devices, depletion modulators have lower modulation efficiency (in the order of 2 V cm) and hence require more energy to operate. For this reason, a longer footprint ($L_{wg} > 1.5$ mm) is needed to reduce this impact, which in turn increases optical loss and complexity of the transmission line design (traveling-wave).

4.3. Carrier injection

Typically, Silicon modulators that use the carrier injection mechanism are based on a *pin* junction [43–48]. The junction is an intrinsic region (represented by *i*) located between the *p* and *n* doping regions with their respective charge carriers, i.e. holes and electrons, respectively. The carriers injection is achieved with forward bias voltage at the *pin* diode. In this way, the electric current flows through the waveguide and the free carriers are brought by the current source, polarizing the diode. In this mechanism, it is important to increase the size of the junction through the intrinsic region, which eliminates excess optical

losses in the waveguide. Fig. 4 shows a modulator that uses the carrier injection principle.

Modulators based on the carrier injection mechanism have low modulation bandwidth, generally in the order of units of MHz. This disadvantage is caused by the slow diffusion of free electrons in the doping zone, which can take several nanoseconds to diffuse over short distances (in the order of micrometers) [73]. To overcome this problem, a pre-emphasis pulse technique applied to the device signal was proposed in [46]. As an example, the modulator proposed in [43] with *pin* junction has a modulation speed of 1.5 Gbit s^{-1}. By applying the pre-emphasis pulse technique to this same structure, the modulator increased modulation speed to 12.5 Gbit s^{-1}. However, the use of pre-emphasis techniques, makes the modulator driver design complex and expensive.

Analyzing Table 1, although some carrier injection modulators have limited modulation speed without the use of pre-emphasis techniques [43,47], they can have high modulation efficiency (e.g. $V_\pi \times L = 0.016$V cm [48]) and hence be manufactured in shorter footprints ($L_{wg} < 0.1$ mm) than depletion devices. In this case, such modulators are notable for consuming lower energy (due to $V_\pi < 1$ V).

4.4. Carrier accumulation

This phenomenon can be implemented using a capacitive structure, with a layer of Poly-Si on the Si waveguide, as shown in Fig. 5. In the state-of-the-art, this type of device is better known as semiconductor–insulator-semiconductor capacitor (SISCAP) [74–77]. The Si and Poly-Si layers are separated by a thin layer of oxide (SiO_2 gate). The use of Poly-Si is compatible with CMOS process and is present on most SOI platforms. Due to its charge carrier mobility be relatively high, polycrystalline Silicon can be easily doped to make electrically active photonic devices. Thus, by applying a voltage to the structure, the majority carriers in the waveguide modify the device refractive index so that a phase change is induced in the optical mode.

The first capacitive modulators were proposed in the middle of the year 2000 [36,37,78]. Based on the carrier accumulation mechanism, such devices have modulation efficiency ($V_\pi \times L$) better than carrier-depletion-based modulators. Therefore, capacitive modulators can be designed with shorter lengths (< 1 mm) and still offer acceptable V_π, behaving as lumped-element, which simplifies its design. Capacitive devices with high dc bias voltage (typically between 2 V and 5 V) is desired for low $V_\pi \times L$. However, it is only possible to to improve bandwidth with low V_{bias}, since low capacitances are achieved in this scenario. It should be noted that, high voltage results in higher optical loss. Although considered for a long time as a promising solution for high-speed applications, it is still challenging to optimize the trade-off between modulation efficiency and bandwidth. This trade-off is related to the oxide gate thickness (t_{gate}). For example, from the study in [16], considering a capacitive modulator with narrower oxide gate thickness (e.g. 5 nm), the $V_\pi \times L$ can be in the order of 0.53 V cm, but with limited bandwidth (~ 20 GHz). On the other hand, increasing the gate thickness to 20 nm, the bandwidth can be improved to > 50 GHz, sacrificing the $V_\pi \times L$ to 2.40 V cm. Therefore, in general, capacitive modulators can not achieve feasible values of $V_\pi \times L$ and f_{3dB} at the same time, and lower SiO_2 gate capacitance (C_{gate}) must be obtained for higher bandwidth (thicker t_{gate}), which penalizes the V_π.

Analyzing Table 1, the design of carrier accumulation modulators [38–41,16,42] optimizes the trade-off between modulation efficiency and modulation speed. For inter-DCI applications, such devices offer acceptable modulation efficiency (in the order of 0.7 V cm) when compared to carrier depletion and carrier injection modulators. Therefore, this structure is very useful for the design of short ($L_{wg} < 1$ mm) and more energy efficient (due to $V_\pi < 7$ V) modulators, without compromising the modulation speed so much (e.g. 40 Gbit s^{-1} [40]).

Several studies tried to improve the capacitive modulators performance through a hybrid integration of Silicon (Si) with other elements, e.g. Indium Phosphide (InP) and Indium Gallium Arsenide Phosphide (InGaAsP). Table 2 shows the state-of-the-art of hybrid modulators based on capacitive effect.

This scheme has less free carriers absorption, resulting in devices with low insertion loss (< 1 dB) when compared to the purely Si & Poly-Si traditional capacitive modulator, which has IL in the order of 8 dB. In addition, in general, the integration of these elements also improved the modulation efficiency (e.g. V_π between 0.86 V and 3.6 V [79–81]), about 10x more than the traditional capacitive structure. However, the bandwidth of these modulators is very low (between 0.1 GHz and 4 GHz) for DCI applications. Although some studies show higher bandwidth (> 25 GHz) [11,12], the V_π becomes unfeasible (> 40 V) for data center interconnect.

Regarding power consumption (see Table 2), a study was performed based on Eqs. (6) and (7). For a fair comparison, the driving voltage (V_D) was set to $V_D = V_\pi$ for scenarios where $V_\pi \leqslant 3.5$ V, since a modulator driver amplifier is not needed [19]. For scenarios where $V_\pi > 6.7$ V, a driving voltage equal to 6.7 V was considered, which is in accordance with the operating threshold of a driver amplifier [21]. Finally, for scenarios where 3.5 V < $V_\pi \leqslant 6.7$ V, a driving voltage equal to V_π was considered, taking into account the use of a driver amplifier. The results show that, the thicker the oxide gate, the lower the SiO_2 gate capacitance and, hence, the lower the power consumption. Therefore, another feature of these modulators is the trade-off between power consumption and modulation efficiency.

Finally, due to the potential to provide significant bandwidth and modulation efficiency, which depend on a physical and geometric device configuration, capacitive modulators are still investigated to provide increasingly efficient FOMs.

5. Conclusion

Despite the wide range of modulators investigated, it is still challenging to propose high-performance, low-cost and simple-design devices for large-scale manufacturing. Hybrid Silicon platforms are considered promising solutions for this purpose, e.g. plasmonic, Lithium Niobate ($LiNbO_3$), Silicon-organic hybrid (SOH), Barium Titanate ($BaTiO_3$), and Graphene. Table 3 summarizes some different alternatives for optical modulation devices that are investigated.

Plasmonic modulators [82,83] feature high confinement in the optical mode, which makes such devices high-efficient (low V_π) in small footprints. However, in general, these modulators employ electro-optical polymer materials that are not compatible with CMOS processes, requiring complex poling. Modulators based on the integration of Si with organic polymers, which use the linear EO effect for modulation, is promising. Silicon-organic hybrid (SOH) modulators, for example, have a high electro-optic tensor coefficient ($n^3 r_{33} > 2000$ pm V^{-1} [92]) and hence provide high modulation efficiency (< 1 V mm) [87]. With slot-type waveguide, such devices have high confinement in the optical

Table 2
State-of-the-art references for hybrid capacitive modulators.

Ref. / Year	[79] 2017	[80] 2017	[81] 2017	[11] 2018	[12] 2019
L_{wg} [μm]	500	250	250	250	250
t_{gate} [nm]	5	10	10	20	20
V_π [V]	0.86	3.5	3.6	40	52
IL [dB]	0.95	~ 1	<1	0.5	0.5
C_{gate} [fF]	~ 3000	NA	NA	>350	>245
f_{3dB} [GHz]	~ 0.1	<2.2	~ 4	>25	30
$E_{bit.C_1}$ [a] [fJ bit^{-1}]	554.7	NA	NA	3928	2750
$E_{bit.C_2}$ [b] [fJ bit^{-1}]	154.1	NA	NA	1091	763.8

[a] $E_{bit.C_1}$ is the power consumption estimated according to Eq. (6).
[b] $E_{bit.C_2}$ is the power consumption estimated according to Eq. (7).

Table 3
Hybrid Silicon modulators.

Platform	Ref.	Year	$V_\pi \times L$ [V mm]	IL [dB]	f_{3dB} [GHz]	L_{wg} [mm]
Si-Plasmonic	[82]	2014	1.3	12	> 65	0.029
Si-$BaTiO_3$-Plasmonic	[83]	2018	0.25	30	> 60	0.010
Si-$LiNbO_3$	[84]	2019	22	2.5	70	5
	[85]	2020	24	18	70	5
SOH	[86]	2014	11	< 2	> 100	0.5
	[87]	2018	1	~ 8	~ 25	1.1
Si-$BaTiO_3$	[88]	2014	15	~ 3.3	0.8	0.75
	[89]	2019	2	NA	2	1
Si-Graphene	[90]	2018	2.8	> 9	5	0.4
	[91]	2018	1.29	NA	NA	0.04

mode. In addition, low chirp, low loss (< 2 dB) and high bandwidth (> 100 GHz) are attractive features of this technology [86]. Due to their low V_π and short interaction length (typically < 1 mm), SOH modulators provide low power consumption, in the order of a few fJ bit^{-1}. Unlike inorganic materials that typically require high temperatures and the use of vacuum equipment, organic materials can be processed at room temperature with lower manufacturing costs. However, similar to other modulation technologies that uses EO polymers, some problems need to be solved, e.g. thermal stability, photochemical stability, time aging process, and photothermal destruction [93].

Conventional Lithium Niobate modulators feature low-index-contrast phase-shifters with weak optical confinement. For this reason, the RF electrodes are designed away from the waveguide to decrease absorption losses, which results in high driving voltage and large footprint. With the Pockels coefficient in integrated form comparable to the bulk form (~ 30 pm V^{-1} [94]), integrated Lithium Niobate modulators have resulted in high bandwidths (70 GHz) [84,85]. Hybrid integration between Si and $LiNbO_3$ has resulted in increasingly efficient and high-speed modulators due to the strong optical confinement resulting from the dry etching manufacturing process. In the state-of-the-art it is possible to find Si-$LiNbO_3$ modulator operating above 100 GHz bandwidth [95], but with limited modulation efficiency (6.7 V cm) due to < 100% vertical coupling of light into the Lithium Niobate layer on top of the Si waveguide. Therefore, still due to the low modulation efficiency compared to other modulation technologies, such devices are manufactured in long lengths (> 5 mm) for low V_π.

Devices based on ferroelectric materials have a strong electro-optical effect. For hybrid integration, Barium Titanate can be epitaxially deposited on Silicon. Due to the high Pockels coefficient (> 1000 pm V^{-1} in bulk form [96]), $BaTiO_3$ modulators offer high modulation efficiency (< 1.5 V cm), but with limited bandwidth (in the order of a few GHz) [88,89]. Speed limitation is mainly associated with parasitic electrical effects [88]. In comparison to the Pockels effect of organic electro-optical materials, such devices provide a slower response. Among the different possible techniques for integrating Barium Titanate into Silicon, molecular beam epitaxy (MBE) [97] stands out for providing a high Pockels coefficient. Because of their high chemical and thermal stability, such modulators are of great interest in the photonics industry.

Ideal for integration into Silicon, graphene is attractive to the photonic industry due to its high optical modulation, high-speed and compatibility with CMOS technologies. Due to their optoelectronic particularities, optical losses in graphene can be suppressed electrically, resulting in modulation of the absorption with a high refractive index change. For the integration of graphene with Silicon, a semi-dry transfer technique is used, allowing a low level of metal contamination during the delamination of graphene from the growth substrate [98]. For electro-absorption and electro-refraction modulation, the physical properties of graphene take advantage over Silicon photonics, since a electro-optical index change > 10^{-3} can be achieved [99], enabling modulation efficiency < 0.3 V cm with short interaction length (< 0.4 mm) [90,91]. However, studies with modulators on this platform are still in a constant stage of evolution for high-speed operation.

Finally, in this paper, an outlook of the main technologies for Silicon (Si) optical modulation was performed. For this, the paper shows the importance of Silicon photonics (SiPh) modulators for the continuous evolution of communication services. To understand the technology bottleneck, figures-of-merit (FOMs) are addressed and serve as a basis for understanding the limiting characteristics of modulators for data center interconnect (DCI) applications. Several notable state-of-the-art studies were considered, where different types of modulators were compared taking FOMs and trade-offs into account. This paper is suitable to better guide researchers regarding problems in Si modulators.

Declaration of Competing Interest

The authors declare that they have no known competing financial interests or personal relationships that could have appeared to influence the work reported in this paper.

References

[1] R.A. Soref, J.P. Lorenzo, Single-crystal silicon: a new material for 1.3 and 1.6 μm integrated-optical components, Electron. Lett. 21 (21) (1985) 953–954, https://doi.org/10.1049/el:19850673.

[2] R. Soref, J. Larenzo, All-silicon active and passive guided-wave components for λ= 1.3 and 1.6 μm, IEEE J. Quantum Electron. 22 (6) (1986) 873–879, https://doi.org/10.1109/JQE.1986.1073057.

[3] R. Soref, Introduction: The Opto-Electronic Integrated Circuit, in: Silicon Photonics, John Wiley & Sons Ltd, The Atrium, Southern Gate, Chichester, West Sussex PO19 8SQ, England, 2008, Ch. 1, pp. 1–14. doi:10.1002/9780470994535.ch1.

[4] Cisco, Global IP Traffic by Application Type, https://www.cisco.com/ (December 2018).

[5] V. Chamola, V. Hassija, V. Gupta, M. Guizani, A Comprehensive Review of the COVID-19 Pandemic and the Role of IoT, Drones, AI, Blockchain, and 5G in Managing its Impact, IEEE Access 8 (2020) 90225–90265.

[6] D.M. Dourado, R.J.L. Ferreira, M. de L. Rocha, U.R. Duarte, Strategies to increase spectral efficiency and energy saving with quality metric assurance in TWDM-PON, Optical Switching Network. 36 (2020) 100550. doi:https://doi.org/10.1016/j.osn.2019.100550.

[7] Yole Développement, Silicon photonics and photonic integrated circuits 2019, Market & Technology Report, http://www.yole.fr/ (April 2019).

[8] E.L. Wooten, K.M. Kissa, A. Yi-Yan, E.J. Murphy, D.A. Lafaw, P.F. Hallemeier, D. Maack, D.V. Attanasio, D.J. Fritz, G.J. McBrien, D.E. Bossi, A review of lithium niobate modulators for fiber-optic communications systems, IEEE J. Sel. Top. Quantum Electron. 6 (1) (2000) 69–82, https://doi.org/10.1109/2944.826874.

[9] J. Ma, J. Yu, C. Yu, X. Xin, X. Sang, Q. Zhang, 64GHz optical millimeter-wave generation by octupling 8GHz local oscillator via a nested LiNbO3 modulator, Optics Laser Technol. 42 (2) (2010) 264–268. doi: 10.1016/j.optlastec.2009.07.002. http://www.sciencedirect.com/science/article/pii/S0030399209001418.

[10] T. Ren, M. Zhang, C. Wang, L. Shao, C. Reimer, Y. Zhang, O. King, R. Esman, T. Cullen, M. Loncar, An Integrated Low-Voltage Broadband Lithium Niobate Phase Modulator, IEEE Photonics Technol. Lett. 31 (11) (2019) 889–892.

[11] S. Menezo, T. Thiessen, P. Grosse, J.K.S. Poon, C. Jany, J.D. Fonseca, B. Szelag, B. Charbonnier, G. El-Zammar, O. Lemonnier, P. Bilondeau, S. Malhouitre, B. Montmayeul, L. Sanchez, High-Speed Heterogeneous InP-on-Si Capacitive Phase Modulators, in: 2018 Optical Fiber Communications Conference and Exposition (OFC), IEEE, San Diego, CA, USA, 2018, pp. 1–3.

[12] T. Thiessen, P. Grosse, J.D. Fonseca, P. Billondeau, B. Szelag, C. Jany, J.k.S. Poon, S. Menezo, 30 GHz heterogeneously integrated capacitive InP-on-Si Mach-Zehnder modulators, Opt. Express 27 (1) (2019) 102–109, https://doi.org/10.1364/OE.27.000102.

[13] J. Wang, C. Qiu, H. Li, W. Ling, L. Li, A. Pang, Z. Sheng, A. Wu, X. Wang, S. Zou, F. Gan, Optimization and Demonstration of a Large-bandwidth Carrier-depletion Silicon Optical Modulator, J. Lightwave Technol. 31 (24) (2013) 4119–4125, https://doi.org/10.1109/JLT.2013.2287671.

[14] Q. Zhang, J. Zhou, J. Hong, A Finite-Difference Time-Domain Large-Signal Model for Silicon Photonics Modulators, IEEE Photonics Technol. Lett. 31 (13) (2019) 1072–1075.

[15] B. Milivojevic, S. Wiese, C. Raabe, A. Shastri, M. Webster, P. Metz, B. Chattin, B. Dama, K. Shastri, Small-size Silicon Photonic IQ modulator and low-power CMOS driver for next generation Coherent Transceivers, in: Proceedings of the 2013 18th European Conference on Network and Optical Communications 2013 8th Conference on Optical Cabling and Infrastructure (NOC-OC I), IEEE, Graz, Austria, 2013, pp. 181–184, https://doi.org/10.1109/NOC-OCI.2013.6582887.

[16] K. Debnath, D.J. Thomson, W. Zhang, A.Z. Khokhar, C. Littlejohns, J. Byers, L. Mastronardi, M.K. Husain, K. Ibukuro, F.Y. Gardes, G.T. Reed, S. Saito, All-silicon carrier accumulation modulator based on a lateral metal-oxide-semiconductor capacitor, Photon. Res. 6 (5) (2018) 373–379, https://doi.org/10.1364/PRJ.6.000373.

[17] M. Raj, Y. Frans, P. Chiang, S.L. Chaitanya Ambatipudi, D. Mahashin, P. De Heyn, S. Balakrishnan, J. Van Campenhout, J. Grayson, M. Epitaux, K. Chang, Design of a 50-Gb/s Hybrid Integrated Si-Photonic Optical Link in 16-nm FinFET, IEEE J. Solid-State Circ. 55 (4) (2020) 1086–1095. doi:10.1109/JSSC.2019.2960487.

[18] 100G Lambda MSA Group, Lambda MSA Group, 400G-FR4 Technical Specification, rev. 2.0 (September 2018).

[19] NeoPhotonics, Driver for Silicon Photonics MZ Modulator to 56 Gbaud, https://www.neophotonics.com/products/56-gbaud-silicon-photonics-driver/ (August 2020).

[20] R.C. Figueiredo, A.L.N. Souza, S.M. Ranzini, A. Chiuchiarelli, Multilevel Pulse Amplitude Modulation Transmissions for Data Center Applications, in: A. Paradisi, R. Carvalho Figueiredo, A. Chiuchiarelli, E. de Souza Rosa (Eds.), Optical Communications: Advanced Systems and Devices for Next Generation Networks, Springer International Publishing, Cham, 2019, pp. 1–16. doi:10.1007/978-3-319-97187-2_1.

[21] A. Balteanu, P. Schvan, S.P. Voinigescu, A 6-bit Segmented DAC Architecture With up to 56-GHz Sampling Clock and 6-Vpp Differential Swing, IEEE Trans. Microw. Theory Tech. 64 (3) (2016) 881–891.

[22] Govind P. Agrawal, Fiber-Optic Communication Systems Third Edition, 3rd ed., John Wiley & Sons, 605 Third Avenue, New York, NY 10158–0012, 2002.

[23] X. Li, F. Yang, F. Zhong, Q. Deng, J. Michel, Z. Zhou, Single-drive high-speed lumped depletion-type modulators toward 10 fJ/bit energy consumption, Photon. Res. 5 (2) (2017) 134–142, https://doi.org/10.1364/PRJ.5.000134.

[24] M. Bass, C. DeCusatis, J. Enoch, V. Lakshminarayanan, G. Li, C. Macdonald, V. Mahajan, E. Van Stryland, Handbook of Optics, Third Edition Volume V: Atmospheric Optics, Modulators, Fiber Optics, X-Ray and Neutron Optics, 3rd ed., McGraw-Hill Inc, USA, 2009.

[25] H. Yu, W. Bogaerts, An Equivalent Circuit Model of the Traveling Wave Electrode for Carrier-Depletion-Based Silicon Optical Modulators, J. Lightwave Technol. 30 (11) (2012) 1602–1609, https://doi.org/10.1109/JLT.2012.2188779.

[26] W. Heinrich, Quasi-TEM description of MMIC coplanar lines including conductor-loss effects, IEEE Trans. Microw. Theory Tech. 41 (1) (1993) 45–52, https://doi.org/10.1109/22.210228.

[27] D. Patel, S. Ghosh, M. Chagnon, A. Samani, V. Veerasubramanian, M. Osman, D. V. Plant, Design, analysis, and transmission system performance of a 41 GHz silicon photonic modulator, Opt. Express 23 (11) (2015) 14263–14287, https://doi.org/10.1364/OE.23.014263.

[28] M.J. Deen, P.K. Basu, Silicon Photonics: Fundamentals and Devices, John Wiley & Sons Ltd, The Atrium, Southern Gate, Chichester, West Sussex PO19 8SQ, England, 2012.

[29] G.T. Reed, G. Mashanovich, F.Y. Gardes, D.J. Thomson, Silicon optical modulators, Nat. Photonics 4 (8) (2010) 518–526, https://doi.org/10.1038/nphoton.2010.179.

[30] P. Dong, S. Liao, D. Feng, H. Liang, D. Zheng, R. Shafiiha, C.-C. Kung, W. Qian, G. Li, X. Zheng, A.V. Krishnamoorthy, M. Asghari, Low V_{pp}, ultralow-energy, compact, high-speed silicon electro-optic modulator, Opt. Express 17 (25) (2009) 22484–22490, https://doi.org/10.1364/OE.17.022484.

[31] C. Koos, J. Leuthold, W. Freude, M. Kohl, L. Dalton, W. Bogaerts, A.L. Giesecke, M. Lauermann, A. Melikyan, S. Koeber, S. Wolf, C. Weimann, S. Muehlbrandt, K. Koehnle, J. Pfeifle, W. Hartmann, Y. Kutuvantavida, S. Ummethala, R. Palmer, D. Korn, L. Alloatti, P.C. Schindler, D.L. Elder, T. Wahlbrink, J. Bolten, Silicon-Organic Hybrid (SOH) and Plasmonic-Organic Hybrid (POH) Integration, J. Lightwave Technol. 34 (2) (2016) 256–268.

[32] W. Heni, Y. Fedoryshyn, B. Baeuerle, A. Josten, C.B. Hoessbacher, A. Messner, C. Haffner, T. Watanabe, Y. Salamin, U. Koch, D.L. Elder, L.R. Dalton, J. Leuthold, Plasmonic IQ modulators with attojoule per bit electrical energy consumption, Nature Commun. 10 (1) (2019) 1694, https://doi.org/10.1038/s41467-019-09724-7.

[33] Y. Zhou, L. Zhou, H. Zhu, C. Wong, Y. Wen, L. Liu, X. Li, J. Chen, Modeling and optimization of a single-drive push–pull silicon Mach-Zehnder modulator, Photon. Res. 4 (4) (2016) 153–161, https://doi.org/10.1364/PRJ.4.000153.

[34] G.T. Reed, A.P. Knights, Silicon-On-Insulator (SOI) Photonics, in: Silicon Photonics, John Wiley & Sons Ltd, The Atrium, Southern Gate, Chichester, West Sussex PO19 8SQ, England, 2005, Ch. 4, pp. 57–110. doi:10.1002/0470014180.ch4.

[35] R. Soref, B. Bennett, Electrooptical effects in silicon, IEEE J. Quantum Electron. 23 (1) (1987) 123–129, https://doi.org/10.1109/JQE.1987.1073206.

[36] A. Liu, R. Jones, L. Liao, D. Samara-Rubio, D. Rubin, O. Cohen, R. Nicolaescu, M. Paniccia, A high-speed silicon optical modulator based on a metal-oxide-semiconductor capacitor, Nature 427 (2004) 615–618.

[37] L. Liao, D. Samara-Rubio, M. Morse, A. Liu, D. Hodge, D. Rubin, U.D. Keil, T. Franck, High speed silicon Mach-Zehnder modulator, Opt. Express 13 (8) (2005) 3129–3135, https://doi.org/10.1364/OPEX.13.003129.

[38] J. Fujikata, S. Takahashi, M. Takahashi, T. Horikawa, High speed and highly efficient Si optical modulator with MOS junction for 1.55m and 1.3m wavelengths, in: 10th International Conference on Group IV Photonics, IEEE, Seoul, South Korea, 2013, pp. 65–66. doi:10.1109/Group4.2013.6644428.

[39] J. Fujikata, M. Noguchi, M. Miura, M. Takahashi, S. Takahashi, T. Horikawa, Y. Urino, T. Nakamura, Y. Arakawa, High performance PIN Ge photodetector and Si optical modulator with MOS junction for photonics-electronics convergence system, in: 2013 18th Asia and South Pacific Design Automation Conference (ASP-DAC), IEEE, Yokohama, Japan, 2013, pp. 655–656. doi:10.1109/ASPDAC.2013.6509674.

[40] M. Webster, P. Gothoskar, V. Patel, D. Piede, S. Anderson, R. Tummidi, D. Adams, C. Appel, P. Metz, S. Sunder, B. Dama, K. Shastri, An efficient MOS-capacitor based silicon modulator and CMOS drivers for optical transmitters, in: 11th International Conference on Group IV Photonics (GFP), IEEE, Paris, France, 2014, pp. 1–2.

[41] D. Perez-Galacho, A. Abraham, S. Olivier, L. Vivien, D. Marris-Morini, Silicon modulator based on interleaved capacitors in sub-wavelength grating waveguides, in: L. Vivien, L. Pavesi, S. Pelli (Eds.), Silicon Photonics and Photonic Integrated Circuits V, vol. 9891, International Society for Optics and Photonics, SPIE, Brussels, Belgium, 2016, pp. 171–176, https://doi.org/10.1117/12.2228843.

[42] M. Douix, D. Perez-Galacho, I. Charlet, C. Baudot, P. Acosta-Alba, S. Kerdilès, C. Euvrard, P. Grosse, J. Planchot, R. Blanc, R. Beneyton, O. Gourhant, S. Crémer, A. Souhaité, N. Vulliet, L. Vivien, D. Marris-Morini, F. Boeuf, SiGe-enhanced Si capacitive modulator integration in a 300 mm silicon photonics platform for low power consumption, Opt. Express 27 (13) (2019) 17701–17707, https://doi.org/10.1364/OE.27.017701.

[43] Q. Xu, B. Schmidt, S. Pradhan, M. Lipson, Micrometre-scale silicon electro-optic modulator, Nature 435 (7040) (2005) 325–327, https://doi.org/10.1038/nature03569.

[44] F. Gan, F.X. Kartner, High-speed silicon electrooptic Modulator design, IEEE Photonics Technol. Lett. 17 (5) (2005) 1007–1009.

[45] W.M.J. Green, M.J. Rooks, L. Sekaric, Y.A. Vlasov, Ultra-compact, low RF power, 10 Gb/s silicon Mach-Zehnder modulator, Opt. Express 15 (25) (2007) 17106–17113, https://doi.org/10.1364/OE.15.017106.

[46] Q. Xu, S. Manipatruni, B. Schmidt, J. Shakya, M. Lipson, 12.5 Gbit/s carrier-injection-based silicon micro-ring silicon modulators, Opt. Express 15 (2) (2007) 430–436, https://doi.org/10.1364/OE.15.000430.

[47] S. Manipatruni, K. Preston, L. Chen, M. Lipson, Ultra-low voltage, ultra-small mode volume silicon microring modulator, Opt. Express 18 (17) (2010) 18235–18242, https://doi.org/10.1364/OE.18.018235.

[48] L. Yang, H. Chen, J. Ding, 12.5 Gb/s carrier-injection silicon Mach-Zehnder optical modulator with high optical bandwidth, in: The 9th International Conference on Group IV Photonics (GFP), IEEE, San Diego, CA, USA, 2012, pp. 129–131.

[49] N.-N. Feng, S. Liao, D. Feng, P. Dong, D. Zheng, H. Liang, R. Shafiiha, G. Li, J. E. Cunningham, A.V. Krishnamoorthy, M. Asghari, High speed carrier-depletion modulators with 1.4V-cm V_πL integrated on 0.25 μm silicon-on-insulator waveguides, Opt. Express 18 (8) (2010) 7994–7999, https://doi.org/10.1364/OE.18.007994.

[50] M. Ziebell, D. Marris-Morini, G. Rasigade, J.-M. Fédéli, P. Crozat, E. Cassan, D. Bouville, L. Vivien, 40 Gbit/s low-loss silicon optical modulator based on a pipin diode, Opt. Express 20 (10) (2012) 10591–10596, https://doi.org/10.1364/OE.20.010591.

[51] P. Dong, L. Chen, C. Xie, L.L. Buhl, Y.-K. Chen, 50-Gb/s silicon quadrature phase-shift keying modulator, Opt. Express 20 (19) (2012) 21181–21186, https://doi.org/10.1364/OE.20.021181.

[52] P. Dong, L. Chen, Y. kai Chen, High-speed low-voltage single-drive push-pull silicon Mach-Zehnder modulators, Opt. Express 20 (6) (2012) 6163–6169, https://doi.org/10.1364/OE.20.006163.

[53] C.T. DeRose, D.C. Trotter, W.A. Zortman, M.R. Watts, High speed travelling wave carrier depletion silicon Mach-Zehnder modulator, in: 2012 Optical Interconnects Conference, IEEE, Santa Fe, NM, USA, 2012, pp. 135–136. doi:10.1109/OIC.2012.6224486.

[54] X. Xiao, H. Xu, X. Li, Z. Li, T. Chu, Y. Yu, J. Yu, High-speed, low-loss silicon Mach-Zehnder modulators with doping optimization, Opt. Express 21 (4) (2013) 4116–4125, https://doi.org/10.1364/OE.21.004116.

[55] J. Zhou, J. Wang, L. Zhu, Q. Zhang, High Baud Rate All-Silicon Photonics Carrier Depletion Modulators, J. Lightwave Technol. 38 (2) (2020) 272–281.

[56] K. Li, S. Liu, D.J. Thomson, W. Zhang, X. Yan, F. Meng, C.G. Littlejohns, H. Du, M. Banakar, M. Ebert, W. Cao, D. Tran, B. Chen, A. Shakoor, P. Petropoulos, G. T. Reed, Electronic-photonic convergence for silicon photonics transmitters beyond 100 Gbps on-off keying, Optica 7 (11) (2020) 1514–1516, https://doi.org/10.1364/OPTICA.411122.

[57] G.B. de Farias, Future Passive Optical Networks: Silicon Photonics based Optical OFDM Solutions, PhD dissertation, Université de Grenoble, 2013.

[58] S.J. Spector, M.W. Geis, M.E. Grein, R.T. Schulein, J.U. Yoon, D.M. Lennon, F. Gan, G. Zhou, F.X. Kaertner, T.M. Lyszczarz, High-speed silicon electro-optical modulator that can be operated in carrier depletion or carrier injection mode, in: 2008 Conference on Lasers and Electro-Optics and 2008 Conference on Quantum Electronics and Laser Science, IEEE, San Jose, CA, USA, 2008, pp. 1–2.

[59] P. Dong, S. Liao, D. Feng, H. Liang, D. Zheng, R. Shafiiha, X. Zheng, G. Li, K. Raj, A. V. Krishnamoorthy, M. Asghari, High speed silicon microring modulator based on carrier depletion, in: 2010 Conference on Optical Fiber Communication (OFC/NFOEC), collocated National Fiber Optic Engineers Conference, IEEE, San Diego, CA, USA, 2010, pp. 1–3. doi:10.1364/NFOEC.2010.JWA31.

[60] D.A. Motta, Y.R.R. Bustamante, A.P. Freitas, G.B. de Farias, U.C. Moura, L.H. Gabrielli, Design of a 40 GHz bandwidth slow-wave silicon modulator, in: 2017 SBMO/IEEE MTT-S International Microwave and Optoelectronics Conference (IMOC), IEEE, Aguas de Lindoia, Brazil, 2017, pp. 1–5.

[61] D.J. Thomson, F.Y. Gardes, J. Fedeli, S. Zlatanovic, Y. Hu, B.P.P. Kuo, E. Myslivets, N. Alic, S. Radic, G.Z. Mashanovich, G.T. Reed, 50-Gb/s Silicon Optical Modulator, IEEE Photonics Technol. Lett. 24 (4) (2012) 234–236.

[62] D. Marris-Morini, X.L. Roux, L. Vivien, E. Cassan, D. Pascal, M. Halbwax, S. Maine, S. Laval, J.M. Fédéli, J.F. Damlencourt, Optical modulation by carrier depletion in a silicon PIN diode, Opt. Express 14 (22) (2006) 10838–10843, https://doi.org/10.1364/OE.14.010838.

[63] Acacia, Acacia Products Overview, https://acacia-inc.com/products/, [Online; accessed March 8, 2020] (2021).

[64] Elenion, Elenion Products Overview, https://elenion.com/products, [Online; accessed March 8, 2020] (2021).
[65] Intel, Intel Products Overview, https://www.intel.com/content/www/us/en/products/network-io/high-performance-fabrics/silicon-photonics.html, [Online; accessed March 8, 2020] (2021).
[66] NeoPhotonics, NeoPhotonics Products Overview, https://www.neophotonics.com/product-category/coherent-transceivers/, [Online; accessed March 8, 2020] (2021).
[67] Alpine Optoelectronics, Alpine Optoelectronics Products Overview, https://www.alpineoptoelectronics.com/?section=products, [Online; accessed March 8, 2020] (2021).
[68] A. Liu, L. Liao, D. Rubin, H. Nguyen, B. Ciftcioglu, Y. Chetrit, N. Izhaky, M. Paniccia, High-speed optical modulation based on carrier depletion in a silicon waveguide, Opt. Express 15 (2) (2007) 660–668, https://doi.org/10.1364/OE.15.000660.
[69] A. Zanzi, C. Vagionas, A. Griol, A. Rosa, S. Lechago, M. Moralis-Pegios, K. Vyrsokinos, N. Pleros, J. Kraft, V. Sidorov, B. Sirbu, T. Tekin, P. Sanchis, A. Brimont, Alignment tolerant, low voltage, 0.23 V.cm, push-pull silicon photonic switches based on a vertical pn junction, Opt. Express 27 (22) (2019) 32409–32426. doi:10.1364/OE.27.032409. http://www.opticsexpress.org/abstract.cfm?URI=oe-27-22-32409.
[70] G.T. Reed, G.Z. Mashanovich, F.Y. Gardes, M. Nedeljkovic, Y. Hu, D.J. Thomson, K. Li, P.R. Wilson, S.-W. Chen, S.S. Hsu, Recent breakthroughs in carrier depletion based silicon optical modulators, Nanophotonics 3 (4–5) (2014) 229–245, https://doi.org/10.1515/nanoph-2013-0016.
[71] M.R. Watts, W.A. Zortman, D.C. Trotter, R.W. Young, A.L. Lentine, Low-Voltage, Compact, Depletion-Mode, Silicon Mach-Zehnder Modulator, IEEE J. Sel. Top. Quantum Electron. 16 (1) (2010) 159–164, https://doi.org/10.1109/JSTQE.2009.2035059.
[72] IMEC, Si-Photonics foundries and technologies, https://europractice-ic.com/, [Online; accessed December 4, 2020] (2020).
[73] M. Lipson, Compact Electro-Optic Modulators on a Silicon Chip, IEEE J. Sel. Top. Quantum Electron. 12 (6) (2006) 1520–1526, https://doi.org/10.1109/JSTQE.2006.885341.
[74] B. Milivojevic, C. Raabe, A. Shastri, M. Webster, P. Metz, S. Sunder, B. Chattin, S. Wiese, B. Dama, K. Shastri, 112 Gb/s DP-QPSK transmission over 2427 km SSMF using small-size silicon photonic IQ modulator and low-power CMOS driver, in: 2013 Optical Fiber Communication Conference and Exposition and the National Fiber Optic Engineers Conference (OFC/NFOEC), OSA, Anaheim, California United States, 2013, pp. 1–3.
[75] M. Webster, C. Appel, P. Gothoskar, S. Sunder, B. Dama, K. Shastri, Silicon Photonic Modulator Based on a MOS-Capacitor and a CMOS Driver, in: 2014 IEEE Compound Semiconductor Integrated Circuit Symposium (CSICS), IEEE, La Jolla, CA, USA, 2014, pp. 1–4.
[76] S. Zhu, G. Lo, Designs of Silicon MIS Phase Modulator With a Deposited AlN Film as the Gate Dielectric, IEEE Photonics Technol. Lett. 27 (11) (2015) 1236–1239.
[77] D.M. Dourado, G.B. de Farias, Y.R.R. Bustamante, M.deL. Rocha, J.P. Carmo, Capacitive Silicon Modulator Design With V-Shaped SiO_2 Gate Waveguide to Optimize V_π×L and Bandwidth Trade-Off, IEEE J. Sel. Top. Quantum Electron. 26 (2) (2020) 1–8, https://doi.org/10.1109/JSTQE.2019.2949464.
[78] K. Shastri, P. Gothoskar, M. Ghiron, V. Patel, R.K. Montgomery, S. Pathak, K.A. Yanushefski, High Speed, Silicon-Based Electro-Optic Modulator, patent US 7,065,301 B2, Jun 2006.
[79] J.-H. Han, F. Boeuf, J. Fujikata, S. Takahashi, S. Takagi, M. Takenaka, Efficient low-loss InGaAsP/Si hybrid MOS optical modulator, Nat. Photonics 11 (2017) 486–491.
[80] T. Hiraki, T. Aihara, K. Hasebe, K. Takeda, T. Fujii, T. Kakitsuka, T. Tsuchizawa, H. Fukuda, S. Matsuo, Heterogeneously integrated III-V/Si MOS capacitor Mach-Zehnder modulator, Nat. Photonics 11 (2017) 482–486.
[81] T. Hiraki, T. Aihara, K. Hasebe, T. Fujii, K. Takeda, T. Kakitsuka, T. Tsuchizawa, H. Fukuda, S. Matsuo, 32-Gbit/s Heterogeneously Integrated Mach-Zehnder Modulator with 250μm-long III-V/Si MOS-capacitor Phase Shifter, in: 2017 European Conference on Optical Communication (ECOC), 2017, pp. 1–3, https://doi.org/10.1109/ECOC.2017.8345866.
[82] A. Melikyan, L. Alloatti, A. Muslija, D. Hillerkuss, P.C. Schindler, J. Li, R. Palmer, D. Korn, S. Muehlbrandt, D. Van Thourhout, B. Chen, R. Dinu, M. Sommer, C. Koos, M. Kohl, W. Freude, J. Leuthold, High-speed plasmonic phase modulators, Nat. Photonics 8 (3) (2014) 229–233, https://doi.org/10.1038/nphoton.2014.9.
[83] A. Messner, F. Eltes, P. Ma, S. Abel, B. Baeuerle, A. Josten, W. Heni, D. Caimi, J. Fompeyrine, J. Leuthold, Integrated Ferroelectric BaTiO3/Si Plasmonic Modulator for 100 Gbit/s and Beyond, in: Optical Fiber Communication Conference, Optical Society of America, 2018, p. M2I.6. doi:10.1364/OFC.2018.M2I.6. http://www.osapublishing.org/abstract.cfm?URI=OFC-2018-M2I.6.
[84] M. He, M. Xu, Y. Ren, J. Jian, Z. Ruan, Y. Xu, S. Gao, S. Sun, X. Wen, L. Zhou, L. Liu, C. Guo, H. Chen, S. Yu, L. Liu, X. Cai, High-performance hybrid silicon and lithium niobate Mach-Zehnder modulators for 100Gbits-1 and beyond, Nat. Photonics 13 (5) (2019) 359–364, https://doi.org/10.1038/s41566-019-0378-6.
[85] S. Sun, M. He, S. Yu, X. Cai, Hybrid Silicon and Lithium Niobate Mach-Zehnder Modulators with High Bandwidth Operating at C-Band and O-Band, in: 2020 Conference on Lasers and Electro-Optics (CLEO), 2020, pp. 1–2.
[86] L. Alloatti, R. Palmer, S. Diebold, K.P. Pahl, B. Chen, R. Dinu, M. Fournier, J.-M. Fedeli, T. Zwick, W. Freude, C. Koos, J. Leuthold, 100 GHz silicon–organic hybrid modulator, Light: Sci. Appl. 3 (5) (2014), https://doi.org/10.1038/lsa.2014.54 e173–e173.
[87] S. Wolf, H. Zwickel, W. Hartmann, M. Lauermann, Y. Kutuvantavida, C. Kieninger, L. Altenhain, R. Schmid, J. Luo, A.K.-Y. Jen, S. Randel, W. Freude, C. Koos, Silicon-Organic Hybrid (SOH) Mach-Zehnder Modulators for 100 Gbit/s on-off Keying, Sci. Rep. 8 (1) (2018) 2598, https://doi.org/10.1038/s41598-017-19061-8.
[88] C. Xiong, W.H.P. Pernice, J.H. Ngai, J.W. Reiner, D. Kumah, F.J. Walker, C.H. Ahn, H.X. Tang, Active Silicon Integrated Nanophotonics: Ferroelectric BaTiO3 Devices, Nano Lett. 14 (3) (2014) 1419–1425, https://doi.org/10.1021/nl404513p.
[89] F. Eltes, C. Mai, D. Caimi, M. Kroh, Y. Popoff, G. Winzer, D. Petousi, S. Lischke, J. E. Ortmann, L. Czornomaz, L. Zimmermann, J. Fompeyrine, S. Abel, A BaTiO3-Based Electro-Optic Pockels Modulator Monolithically Integrated on an Advanced Silicon Photonics Platform, J. Lightwave Technol. 37 (5) (2019) 1456–1462. URL http://jlt.osa.org/abstract.cfm?URI=jlt-37-5-1456.
[90] V. Sorianello, M. Midrio, G. Contestabile, I. Asselberghs, J. Van Campenhout, C. Huyghebaert, I. Goykhman, A.K. Ott, A.C. Ferrari, M. Romagnoli, Graphene-silicon phase modulators with gigahertz bandwidth, Nat. Photonics 12 (1) (2018) 40–44, https://doi.org/10.1038/s41566-017-0071-6.
[91] H. Shu, Z. Su, L. Huang, Z. Wu, X. Wang, Z. Zhang, Z. Zhou, Significantly High Modulation Efficiency of Compact Graphene Modulator Based on Silicon Waveguide, Sci. Rep. 8 (1) (2018) 991, https://doi.org/10.1038/s41598-018-19171-x.
[92] C. Kieninger, Y. Kutuvantavida, D.L. Elder, S. Wolf, H. Zwickel, M. Blaicher, J. N. Kemal, M. Lauermann, S. Randel, W. Freude, L.R. Dalton, C. Koos, Ultra-high electro-optic activity demonstrated in a silicon-organic hybrid modulator, Optica 5 (6) (2018) 739–748, https://doi.org/10.1364/OPTICA.5.000739. URL http://www.osapublishing.org/optica/abstract.cfm?URI=optica-5-6-739.
[93] J. Liu, G. Xu, F. Liu, I. Kityk, X. Liu, Z. Zhen, Recent advances in polymer electro-optic modulators, RSC Adv. 5 (2015) 15784–15794, https://doi.org/10.1039/C4RA13250E.
[94] M. Jacques, A. Samani, D. Patel, E. El-Fiky, M. Morsy-Osman, T. Hoang, M. G. Saber, L. Xu, J. Sonkoly, M. Ayliffe, D.V. Plant, Modulator material impact on chirp, DSP, and performance in coherent digital links: comparison of the lithium niobate, indium phosphide, and silicon platforms, Opt. Express 26 (17) (2018) 22471–22490, https://doi.org/10.1364/OE.26.022471. URL http://www.opticsexpress.org/abstract.cfm?URI=oe-26-17-22471.
[95] P.O. Weigel, J. Zhao, K. Fang, H. Al-Rubaye, D. Trotter, D. Hood, J. Mudrick, C. Dallo, A.T. Pomerene, A.L. Starbuck, C.T. DeRose, A.L. Lentine, G. Rebeiz, S. Mookherjea, Bonded thin film lithium niobate modulator on a silicon photonics platform exceeding 100 GHz 3-dB electrical modulation bandwidth, Opt. Express 26 (18) (2018) 23728–23739, https://doi.org/10.1364/OE.26.023728. URL http://www.opticsexpress.org/abstract.cfm?URI=oe-26-18-23728.
[96] S. Abel, T. Stöferle, C. Marchiori, D. Caimi, L. Czornomaz, M. Stuckelberger, M. Sousa, B.J. Offrein, J. Fompeyrine, A Hybrid Barium Titanate-Silicon Photonics Platform for Ultraefficient Electro-Optic Tuning, J. Lightwave Technol. 34 (8) (2016) 1688–1693, https://doi.org/10.1109/JLT.2015.2510282.
[97] F. Eltes, D. Caimi, F. Fallegger, M. Sousa, E. O'Connor, M.D. Rossell, B. Offrein, J. Fompeyrine, S. Abel, Low-Loss BaTiO3-Si Waveguides for Nonlinear Integrated Photonics, ACS Photonics 3 (9) (2016) 1698–1703, https://doi.org/10.1021/acsphotonics.6b00350.
[98] M.A. Giambra, V. Sorianello, V. Miseikis, S. Marconi, A. Montanaro, P. Galli, S. Pezzini, C. Coletti, M. Romagnoli, High-speed double layer graphene electro-absorption modulator on SOI waveguide, Opt. Express 27 (15) (2019) 20145–20155, https://doi.org/10.1364/OE.27.020145. URL http://www.opticsexpress.org/abstract.cfm?URI=oe-27-15-20145.
[99] M. Romagnoli, V. Sorianello, M. Midrio, F.H.L. Koppens, C. Huyghebaert, D. Neumaier, P. Galli, W. Templ, A. D'Errico, A.C. Ferrari, Graphene-based integrated photonics for next-generation datacom and telecom, Nature Rev. Materials 3 (10) (2018) 392–414, https://doi.org/10.1038/s41578-018-0040-9.